

PROCEEDINGS OF SPIE

SPIDigitalLibrary.org/conference-proceedings-of-spie

Small-scale online simulations in guided-wave photonics

Hammer, Manfred

Manfred Hammer, "Small-scale online simulations in guided-wave photonics," Proc. SPIE 12004, Integrated Optics: Devices, Materials, and Technologies XXVI, 1200414 (5 March 2022); doi: 10.1117/12.2612208

SPIE.

Event: SPIE OPTO, 2022, San Francisco, California, United States

Small-scale online simulations in guided-wave photonics

Manfred Hammer

Paderborn University, Theoretical Electrical Engineering, Paderborn, Germany

ABSTRACT

Online solvers for a series of standard 1-D or 2-D problems in integrated optics will be discussed. Implemented on the basis of HTML/JavaScript/SVG with core routines compiled from well tested C++-sources, the quasi-analytical algorithms require a computational load that can be handled easily even by current mobile devices. So far the series covers the 1-D guided modes of dielectric multilayer slab waveguides and the oblique plane wave reflection from these, the modes of rectangular channel waveguides (in an approximation of effective indices), bend modes of curved multilayer slabs, whispering-gallery resonances (“Quasi-Normal-Modes”) supported by circular dielectric cavities, the hybrid modes of circular multi-step-index optical fibers, bound and leaky modes of 1-D complex multilayers, including plasmonic surface modes, and, with restrictions, quite general rectangular scattering problems in 2-D.

Keywords: online solvers, mode analysis, 1-D/2-D scattering problems, dielectric multilayers, bend modes, whispering gallery resonances, circular optical fibers, leaky modes, surface plasmon polaritons.

1. INTRODUCTION

Current mobile devices provide a computing power that is comparable to the supercomputers of two decades ago.¹ Hence, it should be possible to harness those facilities for highly advanced physical simulations, by the standards of 2000, even if things appear merely small-scale today. With HTML(5) and JavaScript, recent years have seen some standardization,^{2,3} in the encoding of active web-pages, such that it now seems worthwhile to devote effort even to the realization of specialized scientific projects. We illustrate this approach with a series of online tools⁴ for typical low-dimensional problems in computational guided wave photonics.

The solvers are embedded in HTML-pages, with a user-interface encoded in JavaScript, including graphics facilities (inline SVG⁵). For the actual core computations, reasonably mature C++-sources exist.⁶ That codebase includes a couple of routines concerning numerical linear algebra,⁷ and routines for the evaluation of Bessel- and Hankel-functions (of integer order with real arguments,⁷ and for complex order and complex arguments⁸⁻¹⁰). With a respective tool¹¹ these sources are compiled to JavaScript/WebAssembly,¹² and thus become directly available for the online computations. The next Section 2 takes a brief closer look at this computational framework, including some remarks on performance aspects.

Section 3 then provides an overview of our so far existing series of semi-analytical solvers. Roughly, these can be grouped into tools for eigenvalue problems in 1-D (OMS, PlasS, BendS, Sections 3.1–3.3), and 2-D (EIMS, FiMS, WGMs, Sections 3.4–3.6), and scattering problems in 1-D (MuLS, Section 3.7) and 2-D (QuEPS, Section 3.8), for configurations with piecewise constant permittivity, and multilayer slab / rectangular or cylindrical geometry.

2. HTML5 / JAVASCRIPT AS A PLATFORM FOR SMALL-SCALE SCIENTIFIC SIMULATIONS

The online solvers are realized as active web pages; they are executable with any (modern) web browser. The HTML language² is used to create the embedding page. The user interface is directly encoded in JavaScript,³ making use of the manifold HTML form elements. HTML offers graphics facilities e.g. in the form of inline SVG figures.⁵ These are built and can be manipulated programmatically through the script language, but can also be exported as standalone picture files in a high-quality vector format: All (sub-) figures on simulation results in Section 3 have been generated directly by the online solvers, without further editing. Together with CSS style instructions,¹³ the full possibilities of modern web pages become available for the “surface” of the solvers.

M. Hammer, Paderborn University, Theoretical Electrical Engineering, Warburger Straße 100, 33098 Paderborn, Germany,
Phone: ++49 (0)5251/60-3560, Fax: ++49 (0)5251/60-3524, E-mail: manfred.hammer@uni-paderborn.de

Integrated Optics: Devices, Materials, and Technologies XXVI, edited by
Sonia M. García-Blanco, Pavel Cheben, Proc. of SPIE Vol. 12004,
1200414 · © 2022 SPIE · 0277-786X · doi: 10.1117/12.2612208

After accessing the pages and scripts on the server, the solver programs run locally on the user’s machine, the speed depends on the respective hardware. None of the input data is being sent over the internet connection. Note that it is perfectly possible to run these programs from local files; access to a web server is not required for development work on these tools.

With a view to the actual scientific simulations, JavaScript has certain features that do rather not advocate it as a program language, in the first instance: It is an untyped language. The code is interpreted by the web browser (in the first place). Program execution happens in a single thread, together with the browser loop. Local file access is being restricted for security reasons. The language is intended to be error-tolerant (“web pages should not break”).

At a second glance, however, it turns out that many of these apparent drawbacks become less relevant: Suitable development tools are built into all major browsers. Simulation data and figures can be stored locally by “downloading” files. Performance issues concerning computational time and memory are taken care of by automatic optimization and pre-compilation of external code (see next paragraph). Hence, after a certain familiarization period, this framework was experienced actually as rather convenient also for work of a more scientific nature.

Mature C++ routines⁶ were available for the actual core computations of all solvers. These have been *compiled* to JavaScript (a subset, asm.js) / WebAssembly¹² using the “Emscripten” tools.¹¹ Options for optimization exist; the output files are (partly) in a pre-compiled binary runtime format (.wasm) that can be directly digested by the web browsers. Still, execution is limited by the JavaScript environment.

One major issue that remains so far in the present implementation is the single-threadedness. Simulations always take longer than desired, and it is always possible, by cranking up the one or other parameter, to specify an even more complex task. Since the actual computation and the browser loop share the same thread, this then leads to the browser becoming unresponsive (error messages “This page is slowing down . . .”). Some effort has been taken to avoid this issue, in the form of breaking up computations into smaller steps, together with introducing progress bars. For potential future revisions, so far unexploited features in the language (web workers) and in the compiler (thread support) may offer a way out.

Solver	OMS	PlasS	BendS	EIMS	FiMS	WGMs	MuLS	QuEPS
Section, Figure	3.1, 2(a)	3.2, 4	3.3, 6	3.4, 8	3.5, 10	3.6, 12	3.7, 14(a)	3.8, 16
Script/Browser	0.23 s	0.14 s	2.63 s	0.05 s	0.11 s	3.48 s	0.33 s	4.12 s
Native C++	0.18 s	0.09 s	1.48 s	< 0.01 s	0.05 s	1.64 s	0.03 s	1.96 s

Table 1. Runtimes for simulations in the script/browser and for executing an equivalent native compiled program.

Table 1 compares runtimes for simulations of some of the problems considered in Section 3. On the one hand, simulations were carried out in a web-browser (Firefox 94) running the script/precompiled code. On the other hand, the respective C++-sources were compiled (gcc) and executed on the same Linux desktop machine (“native”). One observes time penalty factors script/browser-versus-native-C++ of 2.1 (QuEPS), 1.8 (BendS), and 2.1 (WGMs) for the simulations with less negligible runtimes. Note that the procedures for determining the elapsed time tend to be inaccurate in particular for the present short periods. Also, the internal state of the browser appears to have some (major) influence on the execution time. Nevertheless, the table can give an expression of what to expect; in many cases one receives “instantaneous” results.

3. ONLINE SOLVERS

This concerns eigenvalue or scattering problems in the frequency domain, where the angular frequency $\omega = kc = 2\pi c/\lambda$ and vacuum wavenumber k are specified through the vacuum wavelength parameter λ , for vacuum speed of light c (exception: The WGMs-solver in Section 3.6 determines frequency eigenvalues). The solvers are intended for optical frequencies, and for, in general, nonmagnetic isotropic lossless linear dielectrics. As such, the media are characterized by a relative permeability $\mu = 1$, and spatially dependent but piecewise constant values of real refractive index n and scalar real dielectric permittivity $\epsilon = n^2$ (exception: The PlasS-solver in Section 3.2 accepts complex values for refractive index and permittivity). Facilities for wavelength scans are available for the OMS- and MuLS-solvers in Sections 3.1 and 3.7; here material dispersion is not being taken into account.

3.1 Dielectric multilayer step-index waveguides

OMS: a mode solver for integrated optical dielectric multilayer slab waveguides with 1-D cross sections.¹⁴ For a waveguide definition in terms of refractive indices, layer thicknesses, and a given vacuum wavelength, the script calculates the propagation constants / effective indices of guided modes and allows to inspect the corresponding optical field patterns. Facilities for generating parameter scans are available.

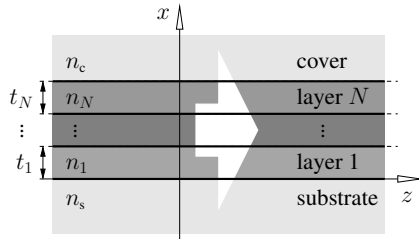


Figure 1. Dielectric multilayer waveguide. A structure with N interior layers is specified in terms of substrate and cladding refractive indices n_s and n_c , and refractive indices n_j and thicknesses t_j , $j = 1, \dots, N$, of the interior layers. Cartesian coordinates x, y, z are oriented such that x is normal to the layer interfaces; the structure is constant along y and z , while all fields are assumed to be constant along y .

2-D multilayer waveguide problems according to Fig. 1 are considered. The solver looks for TE- and TM-polarized electromagnetic fields in the form of slab modes

$$(\mathbf{E}, \mathbf{H})(x, z) = \phi(x) \exp(-i\beta z)$$

that propagate along the z -axis, with mode profiles ϕ , propagation constants $\beta = kN_{\text{eff}}$, and effective indices N_{eff} . The principal field components $\phi = E_y$ and $\phi = H_y$ of TE- and TM-polarized modes satisfy the 1-D Helmholtz equation

$$\partial_x^2 \phi + (k^2 n^2 - \beta^2) \phi = 0$$

within regions with constant refractive index n . Together with the appropriate conditions for continuity of all fields at the dielectric interfaces, and a condition of normalizability, these equations establish an eigenvalue problem for guided modes. A standard transfer matrix technique for dielectric multilayer structures^{15,16} is implemented, with a search for β^2 -eigenvalues on the real axis, driven by nodal properties of principal eigenfields; scenarios with “decoupled” regions are detected and handled appropriately. Fig. 2 shows example results for a silicon slab configuration.

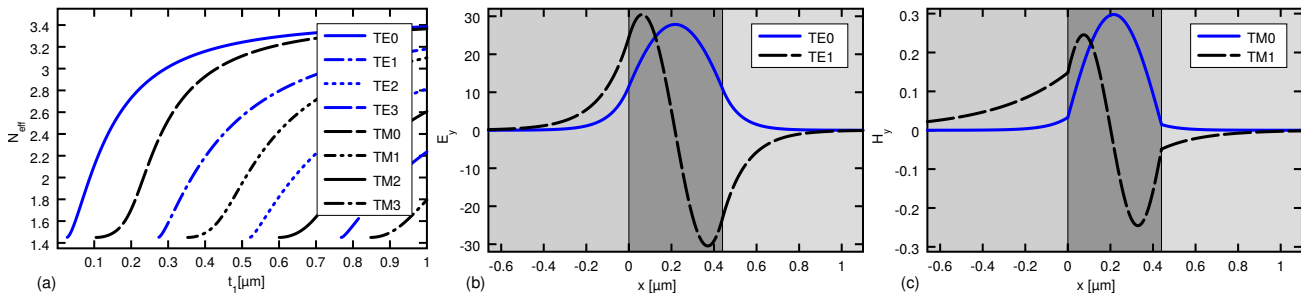


Figure 2. A standard Si/SiO₂ slab waveguide, air cladding, vacuum wavelength $\lambda = 1.55 \mu\text{m}$, refractive indices $n = 1.45, 3.45, 1.0$. Plots: effective indices N_{eff} of guided modes versus the thickness t_1 of the core layer (a), fundamental and first order modes for a layer of thickness $t_1 = 0.44 \mu\text{m}$, principal components E_y and H_y of TE- and TM-modes, respectively (b,c).

3.2 Optical slab waveguides with loss, gain, or leakage

PlasS: an analytic solver for the 1-D eigenmodes of optical multilayer step-index slab waveguides made from media with in general complex refractive index and complex permittivity.¹⁷ Given a potentially guiding configuration defined in terms of refractive index and/or permittivity, layer thicknesses, if applicable, and the vacuum wavelength, the script calculates the complex effective indices of the modes supported by the structure, or their phase propagation and attenuation constants, respectively, and allows to inspect the corresponding optical field patterns. Bound and leaky modes of structures with loss or gain can be identified, as well as the bound solutions related to the propagation of surface-plasmon-polaritons (SPPs) along metal-dielectric interfaces.

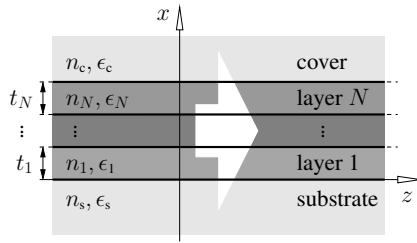


Figure 3. Complex multilayer waveguide, schematically. A structure with N interior layers is specified in terms of substrate and cladding refractive indices n_s and n_c , and refractive indices n_j and thicknesses t_j , $j = 1, \dots, N$, of the interior layers. Alternatively, permittivity values $\epsilon_s, \epsilon_c, \epsilon_j$ can be provided; refractive indices as well as permittivities can be non-real quantities. Cartesian coordinates x, y, z are oriented such that x is normal to the layer interfaces; the structure is constant along y and z , while all fields are assumed to be constant along y .

Complex 2-D waveguide problems according to Fig. 3 are considered. The solver looks for TE- and TM-polarized electromagnetic fields in the form of slab modes

$$(\mathbf{E}, \mathbf{H})(x, z) = \phi(x) \exp(-i\gamma z)$$

that propagate along the z -axis, with mode profiles ϕ , potentially complex propagation constants $\gamma = kN_{\text{eff}} = \beta - i\alpha$, and effective indices N_{eff} , (real) phase propagation constant β and attenuation constant α . The principal field components $\phi = E_y$ and $\phi = H_y$ of TE- and TM-polarized modes satisfy the 1-D Helmholtz equation

$$\partial_x^2 \phi + (k^2 \epsilon - \gamma^2) \phi = 0$$

within regions with constant permittivity ϵ . Together with the appropriate conditions for continuity of all fields at the dielectric interfaces, and a condition of normalizability, these equations establish an eigenvalue problem for bound modes. Alternatively, boundary conditions of exclusively outgoing waves on the outermost layers lead to eigenvalues problems for leaky modes.

A transverse resonance condition can be established by a standard transfer matrix technique for the scalar principal fields. Then valid propagation constants need to be identified as roots of this condition in the complex plane. Initial guesses are generated by considering a “nearby”, truly guiding structure with only the real part of the permittivity profile (note that this well includes the imaginary parts of the complex refractive indices, to some degree). The real propagation constants of bound modes found for these permittivity profiles then serve as starting points for tracing roots in the complex plane, for structures with gradually increasing imaginary parts of the complex permittivity, and/or for gradually increasing refractive index on the outermost layer(s), respectively. In each step, a complex secant method converges the initial guesses numerically to actual roots. Further heuristics are applied for the removal of doublets, and for the classification and ordering of these roots. Fig. 2 shows example results for the short- and long-range surface-plasmon-polariton modes supported by a thin metal layer, for a set of parameters adopted from Ref. 18.

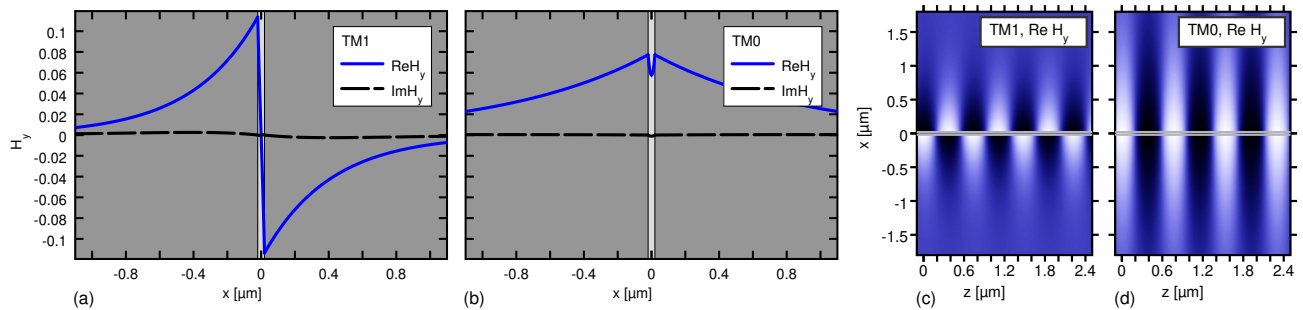


Figure 4. A gold layer of 40 nm thickness, with air cladding, at vacuum wavelength $\lambda = 0.775 \mu\text{m}$, with permittivity $\epsilon = 1.0 : -23.6 - i1.69 : 1.0$ (cf. Ref. 18). The structure supports “short-range” (TM₁, a, c) and “long-range” (TM₀, b, d) surface-plasmon-polariton modes, with effective refractive indices $N_{\text{eff,SR}} = 1.04805 - i5.69 \cdot 10^{-3}$, $N_{\text{eff,LR}} = 1.00976 - i2.77 \cdot 10^{-4}$, and propagation lengths $L_p = 1/(2\alpha)$ of $L_{p,SR} = 10.8 \mu\text{m}$, $L_{p,LR} = 222.3 \mu\text{m}$, respectively. Plots: profiles (a, b) and propagation snapshots (c, d) of the principal magnetic field component H_y .

3.3 Slab waveguide bends

BendS: a mode solver for bent integrated optical dielectric multilayer slab waveguides and curved dielectric interfaces with 1-D cross sections.¹⁹ For a bend configuration defined in terms of bend radius, refractive indices, layer thicknesses, if

applicable, and the vacuum wavelength, the script calculates the complex effective indices of the (leaky) modes supported by the bend, or their phase propagation and attenuation constants, respectively, and allows to inspect the corresponding optical field patterns.

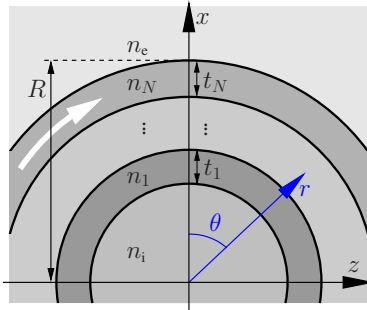


Figure 5. Schematic of a bent waveguide. A structure with N intermediate curved layers is specified in terms of interior and exterior refractive indices n_i and n_e , and refractive indices n_j and thicknesses t_j , $j = 1, \dots, N$, of the intermediate layers. The bend radius R measures the distance from the origin to the outermost interface. Cartesian coordinates x , y , z and cylindrical coordinates r , θ , y are introduced, where x and z , or r and θ , respectively, span the cross sectional plane. The bend structure is constant along θ ; the structure and all fields are assumed to be constant along y .

2-D multilayer bent waveguide problems according to Fig. 5 are considered. The solver looks for TE- and TM-polarized electromagnetic fields in the form of bend modes

$$(\mathbf{E}, \mathbf{H})(r, \theta) = \phi(r) \exp(-i\gamma R\theta)$$

that propagate along the angular direction θ , with mode profiles ϕ , complex propagation constants $\gamma = kN_{\text{eff}}$, and complex effective indices N_{eff} . The principal field components $\phi = E_y$ and $\phi = H_y$ of TE- and TM-polarized modes satisfy the 1-D radial Helmholtz equation

$$\partial_r^2 \phi + r^{-1} \partial_r \phi + (k^2 n^2 - r^{-2} \gamma^2 R^2) \phi = 0$$

within regions with constant refractive index n . Together with the appropriate conditions for continuity of all fields at the dielectric interfaces, and conditions of field regularity at the origin and exclusively outgoing waves in the exterior region, these equations establish an eigenvalue problem for the bend modes.^{9,20}

A transfer matrix technique transforms the radial problem to a transverse resonance condition, roots of which need to be identified in the complex plane. To generate initial estimates, the bend-mode problem is translated to an equivalent straight waveguide problem,¹⁵ followed by feeding restricted staircase approximations of the resulting effective refractive index profiles to the 1-D multilayer slab mode solver of Refs. 6, 14. A complex secant method then converges the initial guesses numerically to actual roots. Further heuristics are applied for the classification and ordering of these solutions. As an example, Fig. 6 shows the three bend modes supported by a nonsymmetric curved slab.

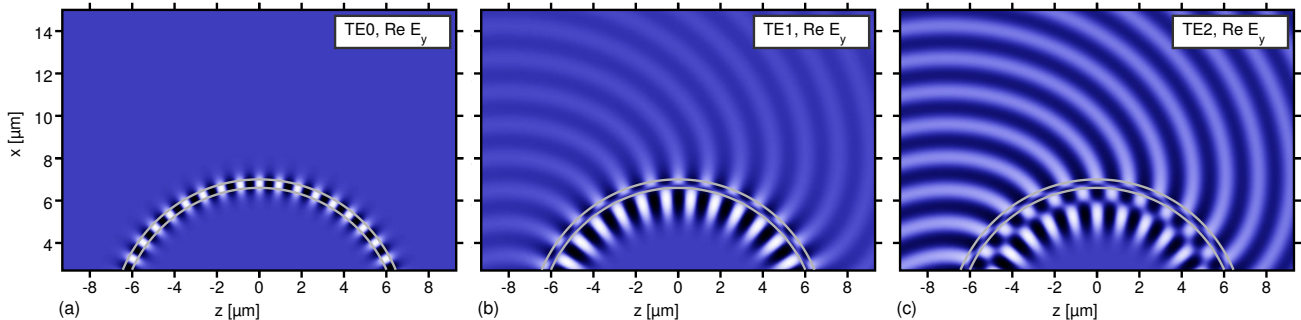


Figure 6. A bent slab waveguide, $\text{SiO}_2/\text{Si}_3\text{N}_4/\text{air}$ layers, index contrast 1.45 : 1.99 : 1.0, core thickness $t_1 = 0.4 \mu\text{m}$, bend radius $R = 7 \mu\text{m}$ (outer rim), TE waves at vacuum wavelength $\lambda = 1.55 \mu\text{m}$. Modes of lowest radial order with effective indices $N_{\text{eff}} = 1.65 - i 1.4 \cdot 10^{-13}$ (TE₀, a), $1.17 - i 2.9 \cdot 10^{-4}$ (TE₁, b), $1.02 - i 6.4 \cdot 10^{-3}$ (TE₂, c); principal electric component E_y , time snapshots.

3.4 Rectangular 2-D waveguides, variational effective index approximation

EIMS: an approximate, semi-analytic mode solver for dielectric integrated optical waveguides with two-dimensional light confinement and weak lateral guiding.²¹ For a waveguide configuration specified in terms of refractive indices, layer

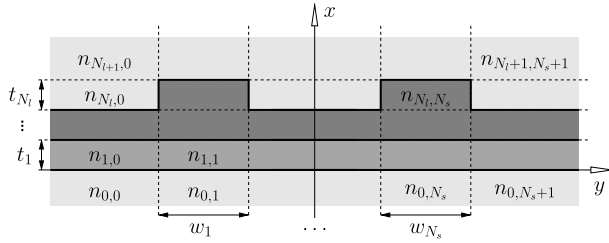


Figure 7. A rectangular waveguide configuration. A structure with N_l inner layers and N_s inner slices is specified in terms of a matrix of refractive indices $n_{l,s}$, $l = 0, \dots, N_l + 1$, $s = 0, \dots, N_s + 1$, thicknesses t_l , $l = 1, \dots, N_l$, of the intermediate layers, and widths w_s , $s = 1, \dots, N_s$, of the inner slices. Cartesian coordinates x, y, z are oriented such that x and y are parallel to the interfaces of slices and layers; the structure is constant along z .

thicknesses, slice widths, and the vacuum wavelength, the script calculates the propagation constants / effective indices of guided modes and allows to inspect the corresponding optical field patterns.

3-D waveguide problems according to Fig. 7 are considered. The solver looks for electromagnetic fields in modal form

$$(\mathbf{E}, \mathbf{H})(x, y, z) = \phi(x, y) \exp(-i\beta z)$$

that propagate along the z -axis, with mode profiles ϕ , propagation constants $\beta = kN_{\text{eff}}$, and effective indices N_{eff} . All components ϕ of the mode profile satisfy the 2-D Helmholtz equation

$$\partial_x^2 \phi + \partial_y^2 \phi + (k^2 n^2 - \beta^2) \phi = 0$$

within all regions with constant refractive index n . Together with the appropriate conditions for continuity of the electromagnetic fields at the dielectric interfaces, and a condition of normalizability, these equations establish a vectorial eigenvalue problem for guided modes.

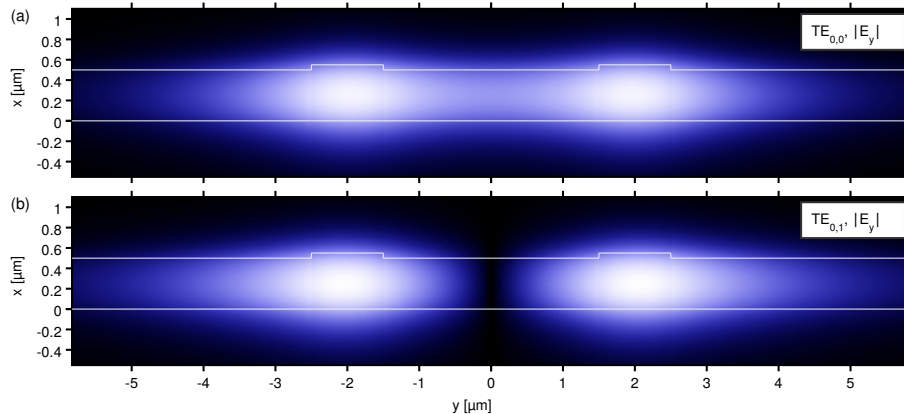


Figure 8. Coupler of two rib waveguides, shallow ribs with thicknesses $t_1 = 0.5 \mu\text{m}$, $t_2 = 0.05 \mu\text{m}$, of widths $w_1 = w_3 = 1 \mu\text{m}$, at a distance of $w_2 = 3 \mu\text{m}$, refractive index contrast 1.45 : 1.99 : 1.0. At wavelength $\lambda = 1.55 \mu\text{m}$, the VEIMS solver identifies two quasi-TE-modes with effective indices $N_{\text{eff}} = 1.77202$ (TE_{0,0}, a) and $N_{\text{eff}} = 1.76965$ (TE_{0,1}, b), and thus predicts a coupling length $L_c = 328 \mu\text{m}$.

The solver then relies on a variational variant of the effective index method²² to reduce things to a series of scalar 1-D eigenvalue problems. More specifically, the script implements what is called VEIM5_{1,0,0,0} (TE) and VEIM5_{0,0,1,0} (TM) in Section 9.2 of Ref. 23; the expressions of Sections 7.1 and 7.2 of Ref. 23 apply. Initially, the solver examines the slab waveguides associated with the refractive index profiles of the interior slices. The slice that supports the guided slab mode with the largest propagation constant is selected as the reference slice. Its guided slab modes serve as potential vertical profiles for the actual 2-D modes. For each of these, the solver computes a lateral effective permittivity profile and determines the 1-D modes supported by this effective permittivity. Those are then used as horizontal profiles for the separable 2-D mode fields. One arrives at semi-vectorial 5-component approximations of the true vectorial modes. Fig. 8 shows example results for a coupler configuration that connects two shallow rib waveguides.

3.5 Circular multi-step index optical fibers

FiMS: an online solver for the guided modes supported by circular dielectric optical fibers with radially piecewise constant refractive index profiles.²⁴ For a fiber defined in terms of (outer) core radius, refractive indices, and thicknesses of

intermediate layers (if applicable), and a specific vacuum wavelength, the script calculates the effective mode indices and propagation constants of the vectorial, hybrid modes supported by the fiber.

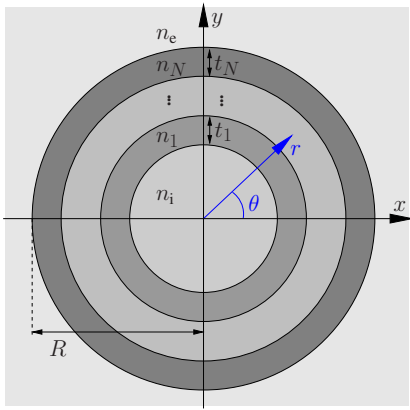


Figure 9. Schematic of a multilayer step-index optical fiber. A circular structure with N intermediate layers is specified in terms of interior and exterior refractive indices n_i and n_e , and refractive indices n_j and thicknesses t_j , $j = 1, \dots, N$, of the intermediate layers. The fiber radius R measures the distance from the origin to the outermost interface. Cartesian coordinates x, y, z and cylindrical coordinates r, θ, y are introduced, where x and z , or r and θ , respectively, span the cross sectional plane. The fiber structure is constant along θ and z .

3-D waveguide problems according to Fig. 9 are considered. The solver looks for electromagnetic fields in modal form

$$(\mathbf{E}, \mathbf{H})(r, \theta, z) = \phi(r) \exp(-il\theta - i\beta z)$$

that propagate along the z -axis, with mode profiles ϕ , integer angular mode order l , propagation constants $\beta = kN_{\text{eff}}$, and effective indices N_{eff} . All components ϕ of the mode profile satisfy the 1-D radial Helmholtz equation

$$\partial_r^2 \phi + r^{-1} \partial_r \phi + (k^2 n^2 - r^{-2} l^2 - \beta^2) \phi = 0$$

within all regions with constant refractive index n . Together with the appropriate conditions for continuity of the electromagnetic fields at the dielectric interfaces, and a condition of normalizability, these equations establish a series of separate vectorial eigenvalue problems for different angular order l , formulated in terms of the principal axial electric and magnetic field components. Following standard theory,^{16,25} the solver applies a transfer matrix technique to establish a transverse resonance condition. Roots are identified by a largely heuristical search procedure on the real axis. As an example, Fig. 10 shows field profiles associated with a series of higher order OAM modes of a silica rod.

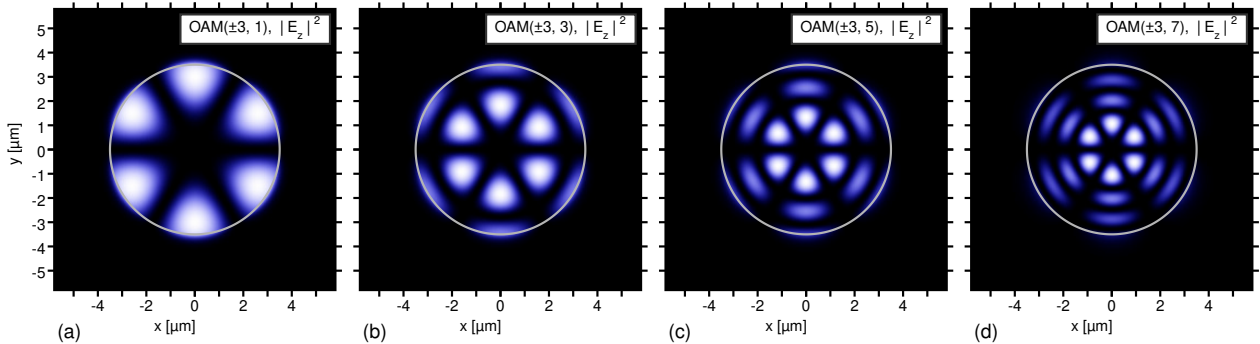


Figure 10. A step-index fiber, refractive index contrast 1.45 : 1.0, rod radius $R = 3.5 \mu\text{m}$. At vacuum wavelength $\lambda = 1.55 \mu\text{m}$, the fiber supports (among several others) the orbital-angular-momentum modes $\text{OAM}(\pm 3, m)$, $m = 1, \dots, 7$ of angular order ± 3 with effective indices N_{eff} of 1.4082 ($m = 1$, a), 1.3349 ($m = 3$, b), 1.2232 ($m = 5$, c), and 1.0705 ($m = 7$, d). The plots show the axial electric field $|E_z|^2$ for superpositions of the degenerate modes $\text{OAM}(-3, m)$ and $\text{OAM}(3, m)$ with unit relative amplitudes.

3.6 Circular dielectric optical cavities

WGMs: an online solver for the whispering gallery resonances of microrings, microdisks, or more general 2-D circular dielectric multilayer cavities in integrated optics / photonics.²⁶ Following the structure definition in terms of cavity radius, refractive indices, and layer thicknesses, if applicable, and the specification of a target vacuum wavelength or of an interval

of potential resonance wavelengths, the script calculates the complex angular eigenfrequencies of the (leaky) whispering gallery modes (WGMs) supported by the cavity, and their resonance wavelengths and linewidths, resonance frequencies, cavity lifetimes, and quality (Q-) factors, respectively.

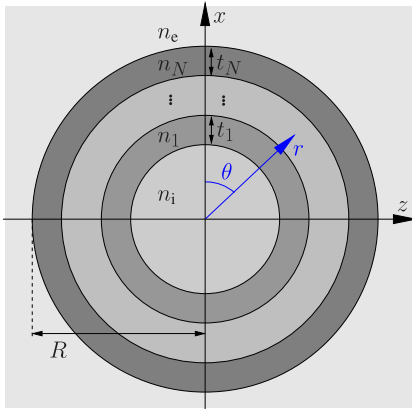


Figure 11. A circular step-index cavity, schematically. A structure with N intermediate layers is specified in terms of interior and exterior refractive indices n_i and n_e , and refractive indices n_j and thicknesses t_j , $j = 1, \dots, N$, of the intermediate layers. The cavity radius R measures the distance from the origin to the outermost interface. Cartesian coordinates x, y, z and cylindrical coordinates r, θ, y are introduced, where x and z , or r and θ , respectively, span the cross sectional plane. The cavity structure is constant along θ ; the structure and all fields are assumed to be constant along y .

Resonance problems for 2-D multilayer cavities according to Fig. 11 are considered. The solver looks for TE- and TM-polarized electromagnetic fields in the form of whispering gallery modes / quasinormal modes

$$(\mathbf{E}, \mathbf{H})(r, \theta, t) = \phi(r) \exp(i\omega_c t - im\theta)$$

of integer angular order m with profile ϕ that oscillate in time with complex eigenfrequency $\omega_c = \omega + i\alpha$, for real resonance frequency ω and attenuation constant α . A resonance wavelength $\lambda = 2\pi c/\omega$ and quality factor $Q = \omega/(2\alpha)$ is associated with each mode. The principal field components $\phi = E_y$ and $\phi = H_y$ of TE- and TM-polarized WGMs satisfy the 1-D radial Helmholtz equation

$$\partial_r^2 \phi + r^{-1} \partial_r \phi + (c^{-2} \omega_c^2 n^2 - r^{-2} m^2) \phi = 0$$

within regions with constant refractive index n . Together with the appropriate conditions for continuity of all fields at the dielectric interfaces, and conditions of field regularity at the origin and exclusively outgoing waves in the exterior region, these equations establish an eigenvalue problem²⁷ for the complex frequency eigenvalue ω_c .

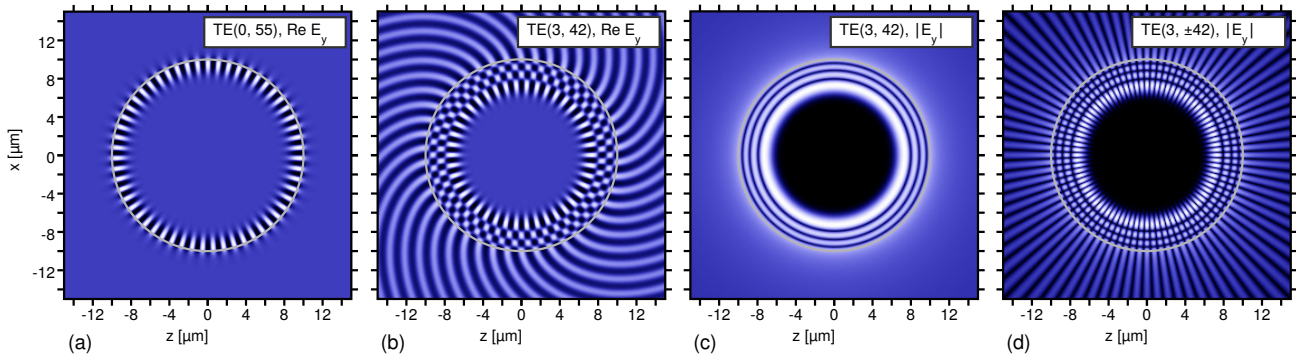


Figure 12. A dielectric disk, refractive index contrast 1.5 : 1.0, radius $R = 10 \mu\text{m}$, TE waves at target vacuum wavelength $\lambda = 1.55 \mu\text{m}$. Plots: whispering gallery modes of specific radial and angular order, with resonance wavelength $\lambda_r = 1.548 \mu\text{m}$ and quality factor $Q = 2.3 \cdot 10^8$ (TE_{0,55}, a), $\lambda_r = 1.538 \mu\text{m}$ and $Q = 1.6 \cdot 10^2$ (TE_{3,42}, b, c, d); time snapshots of the principal E_y field (a, b) and absolute value $|E_y|$ (c, d), for single WGMs (a, b, c) and for a superposition of degenerate modes TE_{3,42} and TE_{3,-42} (d).

A transfer matrix technique transforms the radial problem to a transverse resonance condition, roots of which need to be identified in the complex plane. The solver tries to identify modes with resonance wavelengths that are either close to a target vacuum wavelength, or fall within a specific interval of vacuum wavelengths. To generate initial root estimates, the related bend-mode problem is translated to an equivalent straight waveguide problem,¹⁵ followed by feeding restricted

staircase approximations of the resulting effective refractive index profiles to the 1-D multilayer slab mode solver of Refs. 6, 14. A complex secant method converges these initial guesses numerically to actual roots. Further heuristics are applied for the classification and ordering of these solutions. Fig. 12 illustrates field profiles of two whispering gallery modes supported by a 2-D disk cavity.

3.7 Oblique plane wave incidence on dielectric multilayer stacks

MuLS: a solver for problems of plane wave reflection from dielectric multilayer systems at oblique incidence.²⁸ Given the stack definition in terms of refractive indices, layer thicknesses, vacuum wavelength, and the angle of incidence, the script calculates reflectance and transmittance properties for s- and p-polarized waves, and allows to inspect the corresponding optical fields. Facilities for evaluating parameter scans / spectra are available. The script can serve as a basic tool for the design of dielectric multilayer coatings / reflectors / filters.

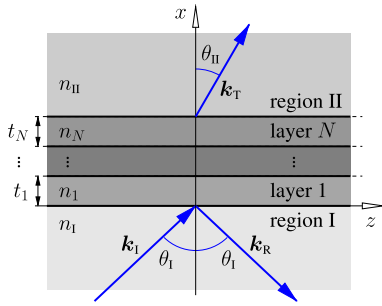


Figure 13. A dielectric multilayer stack. Incoming and reflected waves are present in exterior region I, propagating at angles θ_I . Transmitted waves are observed in exterior region II at angle θ_{II} . A structure with N interior layers is specified in terms of refractive indices n_1 and n_{II} on the input and exit side, and refractive indices n_j and thicknesses t_j , $j = 1, \dots, N$, of the interior layers. Cartesian coordinates x, y, z are oriented such that x is normal to the layer interfaces; the structure is constant along y and z . All fields are assumed to be constant along y , the x - and z -axes span the plane of incidence.

2-D problems of plane wave reflection from a dielectric multilayer stack are considered, as shown in Fig. 13. For given angle of incidence θ_I and respective wavenumber $k_{1,z} = kn_I \sin \theta_I$, the solver computes perpendicularly s/TE- and parallel p/TM-polarized electromagnetic fields of the form

$$(\mathbf{E}, \mathbf{H})(x, z) = \phi(x) \exp(-ik_{1,z}z)$$

with profile function ϕ . The principal field components $\phi = E_y$ and $\phi = H_y$ of s/TE- and p/TM-polarized solutions satisfy the 1-D Helmholtz equation

$$\partial_x^2 \phi + (k^2 n^2 - k_{1,z}^2) \phi = 0$$

within regions with constant refractive index n . Together with the appropriate conditions for continuity of all fields at the dielectric interfaces, and a condition of only outgoing reflected and transmitted waves in regions I and II, respectively, these equations establish the linear scattering problem. A standard transfer matrix technique for dielectric multilayer structures²⁹ is applied to solve this system for internal field solutions, for the associated reflection and transmission coefficients, and for reflectance and transmittance values, respectively. Fig. 2 shows example results for a multilayer Bragg reflector with a defect cavity at its center.

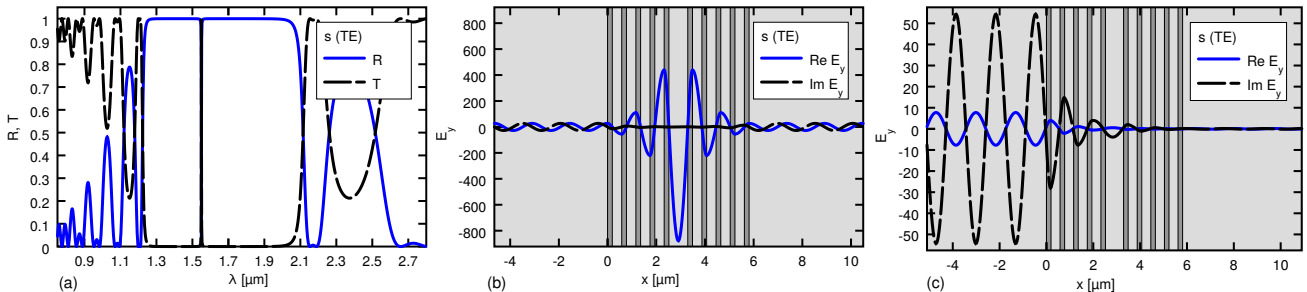


Figure 14. A Bragg-resonator with 19 interior layers, with refractive indices $n = 1, 2, 1, 2, \dots, 2, 1$ and quarter-wave thicknesses $t_i = \lambda/(4n_i)$, with a central cavity layer of thickness $t_{10} = \lambda/(2n_{10})$. Normal incidence $\theta_I = 0^\circ$ of waves at target wavelength $\lambda = 1.55 \mu\text{m}$ is considered. Plots: transmittance T and reflectance R versus wavelength λ (a), field profiles E_y at $\lambda = 1.55 \mu\text{m}$, at resonance (b), and at $\lambda = 1.7 \mu\text{m}$, off-resonance, in the reflectance bandgap (c).

3.8 Rectangular optical guided-wave scattering problems

QuEPS: The scalar polarized 2-D Helmholtz equations are addressed, on a rectangular computational domain with transparent boundary conditions that permit guided wave in- and outflux. Given a problem specification in terms of interface positions, a matrix of refractive index values, polarization and wavelength parameters, and guided wave input, the script³⁰ determines modal output amplitudes (elements of the scattering matrices), and the power levels associated with guided and unguided directional outgoing waves (transmittances / reflectances, power balance).

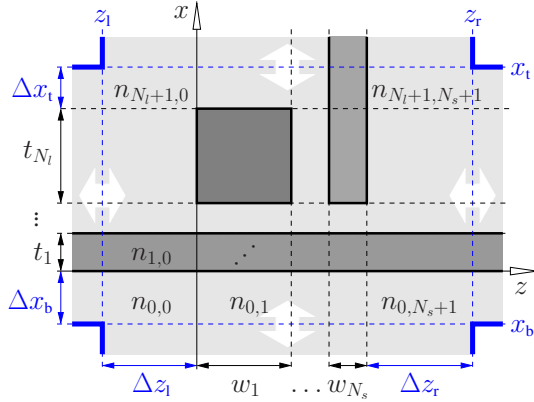


Figure 15. Schematic of the rectangular scattering problems. A structure with N_1 inner layers and N_s inner slices is specified in terms of a matrix of refractive indices $n_{l,s}$, $l = 0, \dots, N_1 + 1$, $s = 0, \dots, N_s + 1$, thicknesses t_l , $l = 1, \dots, N_1$, of the intermediate layers, and widths w_s , $s = 1, \dots, N_s$, of the inner slices. Cartesian coordinates x, y, z are oriented such that x and z are parallel to the interfaces of slices and layers; the structure and all fields are assumed to be constant along y . The solver works on a cross-shaped computational domain, with an inner rectangular computational window $(x, z) \in [x_b, x_t] \times [z_1, z_r]$. The window is set by the distances $\Delta x_b, \Delta x_t, \Delta z_1, \Delta z_r$ between the outermost interface positions, and the boundary locations.

Rectangular guided wave scattering problems according to Fig. 15 are considered. Individual amplitudes can be specified for incoming guided modes that are supported by the channels on all four sides of the inner computational window. The solver then computes electromagnetic fields $(\mathbf{E}, \mathbf{H})(x, z)$ as functions of the cross sectional coordinates x, z , where the principal components E_y of TE- and H_y of TM-polarized fields satisfy the 2-D Helmholtz equation

$$\partial_x^2 \phi + \partial_z^2 \phi + k^2 n^2 \phi = 0$$

within all regions with constant refractive index n . Together with the appropriate conditions for continuity of the electromagnetic fields at the dielectric interfaces, and conditions of only outgoing waves in the exterior regions of the cross-shaped computational domain (beyond the given incoming modes), these equations establish the linear scattering problem.

The solver follows an algorithm for quadridirectional eigenmode propagation (QUEP).³¹ The electromagnetic field is expanded into the sets of normal modes (1-D slab modes with Dirichlet boundary conditions) supported by the refractive index profiles associated with the layers and slices that make up the circuit. Inside the inner computational window, quadridirectional expansions into modes that propagate in the $\pm x$ - and $\pm z$ -directions apply. Bidirectional expansions in the half-infinite exterior regions ensure that the boundaries of the inner window become transparent for outgoing (scattered) waves from the interior. The system is solved for the full interior field solution, for the associated output amplitudes of guided modes on all outgoing channels, and for the outgoing power fractions that traverse the boundaries of the inner computational window. Figs. 16 and 17 show results of simulations of a waveguide facet and of a rectangular resonator circuit.³¹

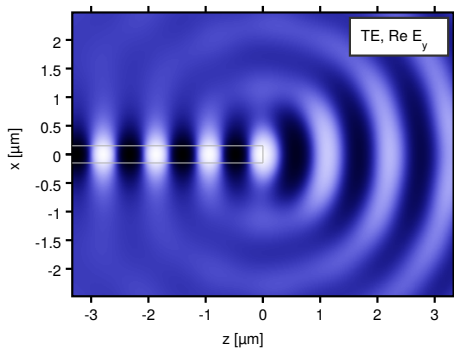


Figure 16. Facet of a slab waveguide, a Si_3N_4 -core ($n = 1.99$) of thickness $t_1 = 0.3 \mu\text{m}$ surrounded by SiO_2 ($n = 1.45$). Incidence of the guided TE_0 -wave at vacuum wavelength $\lambda = 1.55 \mu\text{m}$ leads to about 2% reflectance. QUEP-computation with 124×133 spectral terms, $(x_t - x_b) \times (z_r - z_1) = 9.6 \times 10.3 \mu\text{m}^2$. Plot: snapshot of the principal TE component E_y .

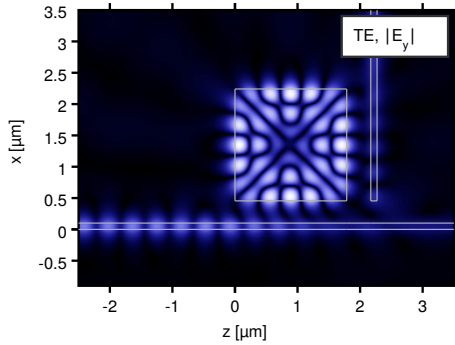


Figure 17. A square 2-D microresonator with perpendicular port waveguides, cores of thickness $t_1 = w_3 = 0.1 \mu\text{m}$, separated by gaps $t_2 = 0.355 \mu\text{m}$, $w_2 = 0.385 \mu\text{m}$ from the cavity of dimension $w_1 \times t_3 = 1.786 \mu\text{m}^2$, index contrast 3.4 : 1.0; TE₀-excitation from the left at $\lambda = 1.55 \mu\text{m}$, guided output power 22% (left), 46% (top), 22% (right). QUEP-computation 133×133 spectral terms, $(x_t - x_b) \times (z_r - z_l) = 10.2 \times 10.3 \mu\text{m}^2$. Plot: principal TE component E_y , absolute value.

4. CONCLUDING REMARKS

A series of online solvers for small-scale eigenvalue and scattering problems in guided wave photonics are discussed. These are realized in a framework of HTML web pages, with active content coded in JavaScript, and optimized core routines compiled from established external sources (here C++). We observed penalty factors of about 2 in computational time, when comparing the scripts running in a web browser with executables compiled specifically for the respective machine. The solvers generate directly figures as shown in the preceding sections. Where appropriate, facilities for time-animation of complex frequency-domain fields are provided, in the form of repeated loops over one time period. The programs might be viewed as examples for the possibilities offered by the HTML/JavaScript/SVG framework for the online dissemination of academic simulation tools.

On the one hand, in a context of scientific simulations, this web-centered environment has certain shortcomings, mostly related to the particularities of the program language, and to security restrictions required for external web pages. On the other hand, all the burdens (compatibility, installation, distribution) that otherwise might prevent the use of an academic simulation tool by “others” are entirely absent. Our programs have proven to be particularly useful for purposes of demonstration and teaching, but just as well for other, more “serious” tasks in integrated photonics design. All solvers are free to use, available online at <https://www.siiio.eu>.

ACKNOWLEDGMENTS

The author thanks Lena Ebers and Jens Förstner for many fruitful discussions, and for valuable comments on the manuscript. Financial support from the German Research Foundation (Deutsche Forschungsgemeinschaft DFG, project 231447078–TRR 142, subproject C05) is gratefully acknowledged.

REFERENCES

- [1] Dongarra, J. and Luszczek, P., “Anatomy of a globally recursive embedded LINPACK benchmark,” in [2012 IEEE Conference on High Performance Extreme Computing], 1–6 (2012). (Presentation available).
- [2] Web Hypertext Application Technology Working Group (WHATWG), “HTML Living Standard.” <https://html.spec.whatwg.org/>.
- [3] Ecma International, Geneva, Switzerland, “ECMA-262 — ECMAScript 2021 language specification.” <https://www.ecma-international.org/publications-and-standards/standards/ecma-262/>.
- [4] Hammer, M., “Simulations in Integrated Optics, online solvers.” <https://www.siiio.eu/>.
- [5] World Wide Web Consortium (W3C), “Scalable Vector Graphics (svg), open standard.” <https://www.w3.org/Graphics/SVG/>.
- [6] Hammer, M., “METRIC — Mode expansion tools for 2D rectangular integrated optical circuits.” <https://metric.computational-photonics.eu/>.
- [7] Press, W. H., Teukolsky, S. A., Vetterling, W. T., and Flannery, B. P., [Numerical Recipes in C, 2nd ed.], Cambridge University Press (1992).
- [8] Kodama, M., “Algorithm 912: A module for calculating cylindrical functions of complex order and complex argument,” *ACM Transactions on Mathematical Software* **37**(4) (2011).

- [9] Hiremath, K. R., [*Coupled Mode Theory Based Modeling and Analysis of Circular Optical Microresonators*], University of Twente, Enschede, The Netherlands (2005). Ph.D. Thesis.
- [10] Amos, D. E., “A portable package for Bessel functions of a complex argument and nonnegative order.” <http://www.netlib.org/amos/>.
- [11] The Emscripten Community, “Emscripten, Compiling to asm.js and WebAssembly.” <https://emscripten.org/>.
- [12] World Wide Web Consortium (W3C), “Webassembly.” <https://webassembly.org/>.
- [13] World Wide Web Consortium (W3C), “Cascading Style Sheets (CSS) style sheet language.” <https://www.w3.org/TR/CSS/>.
- [14] Hammer, M., “OMS — 1-D mode solver for dielectric multilayer slab waveguides.” <https://www.computational-photonics.eu/oms.html>.
- [15] Vassallo, C., [*Optical Waveguide Concepts*], Elsevier, Amsterdam (1991).
- [16] Okamoto, K., [*Fundamentals of Optical Waveguides*], Academic Press, San Diego (2000).
- [17] Hammer, M., “PlasS — 1-D mode solver for complex optical multilayer step-index slab waveguides.” <https://www.computational-photonics.eu/plass.html>.
- [18] Bozhevolnyi, S. I. and Søndergaard, T., “General properties of slow-plasmon resonant nanostructures: nano-antennas and resonators,” *Optics Express* **15**(17), 10869–10877 (2007).
- [19] Hammer, M., “BendS — 1-D mode solver for slab waveguide bends.” <https://www.computational-photonics.eu/bends.html>.
- [20] Hiremath, K. R., Hammer, M., Stoffer, R., Prkna, L., and Čtyroký, J., “Analytical approach to dielectric optical bent slab waveguides,” *Optical and Quantum Electronics* **37**(1-3), 37–61 (2005).
- [21] Hammer, M., “EIMS — 2-D multilayer waveguide mode solver, variational effective index approximation.” <https://www.computational-photonics.eu/eims.html>.
- [22] Ivanova, O. V., [*Dimensionality Reduction in Computational Photonics*], University of Twente, Enschede, The Netherlands (2010). Ph.D. Thesis.
- [23] Ivanova, O. V., Stoffer, R., and Hammer, M., “A variational mode solver for optical waveguides based on quasi-analytical vectorial slab mode expansion,” (2013). arXiv:1307.1315v2 [physics.optics].
- [24] Hammer, M., “FiMS — Modes of circular multi-step index optical fibers.” <https://www.computational-photonics.eu/fims.html>.
- [25] Snyder, A. W. and Love, J. D., [*Optical Waveguide Theory*], Chapman and Hall, London, New York (1983).
- [26] Hammer, M., “WGMs — Whispering gallery modes of circular 2-D dielectric optical cavities.” <https://www.computational-photonics.eu/wgms.html>.
- [27] Franchimon, E. F., Hiremath, K. R., Stoffer, R., and Hammer, M., “Interaction of whispering gallery modes in integrated optical micro-ring or -disk circuits: Hybrid CMT model,” *Journal of the Optical Society of America B* **30**(4), 1048–1057 (2013).
- [28] Hammer, M., “MULS — Oblique incidence of plane waves on dielectric multilayer stacks.” <https://www.computational-photonics.eu/muls.html>.
- [29] Born, M. and Wolf, E., [*Principles of Optics, 7th. ed.*], Cambridge University Press, Cambridge, UK (1999).
- [30] Hammer, M., “QuEPS — 2-D frequency domain solver for rectangular optical guided-wave scattering problems.” <https://www.computational-photonics.eu/queps.html>.
- [31] Hammer, M., “Quadrirectional eigenmode expansion scheme for 2-D modeling of wave propagation in integrated optics,” *Optics Communications* **235**(4–6), 285–303 (2004).